

Article

The Interplay of Thermal Gradient and Laser Process Parameters on the Mechanical Properties, Geometrical and Microstructural Characteristics of Laser-Cladded Titanium (Ti6Al4V) Alloy Composite Coatings

Olawale Samuel Fatoba * and Tien-Chien Jen 

Department of Mechanical Engineering Science, University of Johannesburg, Johannesburg 2006, South Africa; tjen@uj.ac.za

* Correspondence: proffatobasameni@gmail.com

Abstract: With the development of laser surface modification techniques like direct laser metal deposition (DLMD), titanium alloy (Ti6Al4V) may now have its entire base metal microstructure preserved while having its surface modified to have better characteristics. Numerous surface issues in the aerospace industry can be resolved using this method without changing the titanium alloy's primary microstructure. As a result, titanium alloy is now more widely used in sectors outside of aerospace and automotive. This is made possible by fabricating metal composite coatings on titanium alloys using the same DLMD method. Any component can be repaired using this method, thereby extending the component's life. The experimental process was carried out utilizing a 3000 W Ytterbium Laser System at the National Laser Centre of the CSIR in South Africa. Through the use of a laser system, AlCuTi/Ti6Al4V was created. The characterization of the materials for grinding and polishing was performed according to standard methods. There is a substantial correlation between the reinforcement feed rate, scan speed, and laser power components. Due to the significant role that aluminum reinforcement played and the presence of aluminum in the base metal structure, Ti-Al structures were also created. The reaction and solidification of the copper and aluminum reinforcements in the melt pool produced the dendritic phases visible in the microstructures. Compared to the base alloy, the microhardness's highest value of 1117.2 HV_{1.0} is equivalent to a 69.1% enhancement in the hardness of the composite coatings. The enhanced hardness property is linked to the dendritic phases formed in the microstructures as a result of optimized process parameters. Tensile strengths of laser-clad ternary coatings also improved by 23%, 46.2%, 13.1%, 70%, 34.3%, and 51.7% when compared to titanium alloy substrates. The yield strengths of laser-clad ternary coatings improved by 19%, 46.7%, 12.9%, 69.3%, 34.7%, and 52.1% when compared to the titanium alloy substrate.

Keywords: titanium alloy (Ti6Al4V); ternary coatings; laser cladding; microstructure; geometrical characteristics; mechanical properties



Citation: Fatoba, O.S.; Jen, T.-C. The Interplay of Thermal Gradient and Laser Process Parameters on the Mechanical Properties, Geometrical and Microstructural Characteristics of Laser-Cladded Titanium (Ti6Al4V) Alloy Composite Coatings. *Metals* **2023**, *13*, 1617. <https://doi.org/10.3390/met13091617>

Academic Editors: Aleksander Lisiecki and Antonio Riveiro

Received: 29 June 2023

Revised: 5 September 2023

Accepted: 14 September 2023

Published: 19 September 2023



Copyright: © 2023 by the authors. Licensee MDPI, Basel, Switzerland. This article is an open access article distributed under the terms and conditions of the Creative Commons Attribution (CC BY) license (<https://creativecommons.org/licenses/by/4.0/>).

1. Introduction

There is a growing need for materials that perform well in corrosive and extreme wear environments, which has led to the development of several surface treatment procedures [1]. Corrosion, wear, and fatigue attacks are common problems for many engineering materials used in industrial settings, which cause the material's surface to deteriorate quickly. Hard coatings are applied to materials in order to save expenses, save energy, and preserve raw materials because of these factors [2]. Surface improvement of engineering materials can be used to avoid and control degradation and service failure in industries. However, conventional surface modifications and coatings are inadequate to meet the demands of a material surface in conditions that are corrosive and subject to wear.

In reality, using old technologies led to higher costs, wasted time, and the inability to fix manufacturing errors. There are several factors that influence the surface quality of additive manufacturing, such as material selection, build direction, orientation, and process parameters. The aerospace sector will be able to fully leverage additive manufacturing technologies once these problems are fixed. These benefits have led to the majority of manufacturing industries (more than 60%) considering additive manufacturing for the creation of their products and component parts. Aluminum alloy and additive manufacturing together allowed for a 60% weight reduction in aviation engines. These reports indicate that strength, tiredness, and endurance did not change. In a similar vein, only 10% of the raw materials are needed when titanium alloys are used in additive manufacturing to produce aerospace engines. While additive manufacturing offers certain benefits over conventional methods, it also has certain drawbacks. Among other things, it is crucial to take into account the build speed, precision, post-processing, orientation of the pieces, material qualities, and surface quality when utilizing the additive manufacturing method. High-quality parts cannot be manufactured until a deep understanding of technology and material design is entrenched. The aforementioned process parameters need to be optimized for these, and material selection needs to be well thought out.

Highly corrosion-resistant metallic surfaces can be created using a variety of laser surface treatment techniques, the most commonly utilized being laser surface melting, laser cladding, and laser surface alloying [3]. With laser cladding, the near-surface structure and surface morphology of parts and clads that stick perfectly to the bulk steel interface can be changed. Kwok et al. [4], Dobrzanski et al. [5], and Wei et al. [6] stated that the main benefits of this technique for surface modification are that it can make meta-stable structures with new properties that cannot be made with other methods and that it can reduce grain size because it has a fast quench rate. On the matrix, a dependable coating devoid of pores and cracks can be created with the right laser processing settings [7]. Because of the significant temperature differences between the melted surface area and the solid substrate beneath, this causes the new alloy to self-quench and resolidify quickly [8,9]. Poulon-Quintina et al. [10] stated that some microstructures, such as metastable phases and nano-crystalline grains, can be produced by laser beams due to unique thermal properties brought about by laser irradiation. Thus, by depositing a premixed ratio of constituent powders, a new alloy can be synthesized during the laser cladding process [11].

Due to the intricate and essential parts of an airplane, the aerospace sector is expected to benefit more from the effects of additive manufacturing technology in the twenty-first century [12,13]. However, due to limitations on surface quality, additive manufacturing has only been partially adopted and used in the aerospace industry. Structural integrity, materials control, limits on design variables, dependability, maintainability, production sustainability, and cost factor are only a few of the problems that continue to prevent additive manufacturing from becoming fully inclusive in the aerospace industry [14,15]. In addition, the surface quality of the manufactured parts is one of the main limitations of additive manufacturing, and numerous studies have discussed these problems [16–18]. Conventional technologies have been used to close the gap despite these problems, but they are ineffective [19]. The traditional technologies even resulted in cost increases, time wastage, and the inability to correct mistakes made during manufacturing.

Due to qualities like low density, excellent corrosion resistance, high specific strength, low elastic modulus, and biocompatibility, titanium alloy has found extensive use in the marine, aerospace, medical, and automotive industries [20,21]. Some researchers found that titanium alloy composite coatings with laser cladding had small heat-affected zones, improved microstructures, little stress deformation, and excellent bonding [22,23]. Despite all of the remarkable qualities of titanium alloy, low hardness and weak wear resistance have been significant problems [24]. Numerous researchers have altered the properties of titanium alloys using composite coatings such as metal matrix composites, polymer matrix composites, and ceramic matrix composites [25–27]. With the development of laser surface modification techniques like direct laser metal deposition (DLMD), titanium alloy

(Ti6Al4V) may now have its entire base metal microstructure preserved while having its surface modified to have better characteristics. Numerous surface issues in the aerospace industry can be resolved using this method without changing the titanium alloy's primary microstructure. As a result, titanium alloy is now more widely used in sectors outside of aerospace and automotive.

According to Yang [28], microstructure and wear resistance exhibit a decline in characteristics under high and excessive dilution. This causes deformation and lingering strains that might cause microcracks in the laser deposition process. Based on the energy of the laser beam absorbed by the base alloy substrate, substrate geometry, beam profile, laser beam spot size, and material properties, the depth of dilution in the melt pool is determined. The beam power density depends on both the laser power and the spot area. According to Gharehbaghi et al. [29], the degree of dilution, the width of the clad deposit, and the efficiency of the powder can all rise as the laser power does. As a result of diluting the substrate (base alloy), the author further found that the cladding height can also be decreased by continuously increasing laser power. It indicates that the cladding height starts to drop when the melting of reinforced materials in the melt pool starts. The authors came to the conclusion that this was caused by the base alloy surface receiving more energy, which in turn caused an increase in molten powder. If more energy is supplied than is necessary, the melt pool may vaporize, and a keyhole may form as a result.

The main aim of this work is to design and fabricate novel advanced metallic coatings with improved mechanical properties and microstructural evolution using laser surface modification technique.

2. Materials and Method

The base alloy specimen, as seen in Table 1, was dimensioned and cut to $80 \times 80 \times 5 \text{ mm}^3$. Standard techniques were used on each specimen to reveal the microstructural evolution of the samples. The experimental process was conducted at the National Laser Centre, CSIR, South Africa, utilizing a 3000 W Ytterbium Laser System (YLS).

Table 1. Base metal chemical composition (Ti-6Al-4V Alloy).

Elements	Ti	Al	V	Fe	O	C	N
Wt.%	Bal.	6.2	3.9	0.2	0.01	0.12	0.005

In Figure 1a, a 3 kW continuous-wave ytterbium laser system (YLS) is shown connected to a KUKA robot that controls the mobility of the cladding process. The laser beam is directed toward the optical system's focusing lenses by the optical fiber through which it is moving. The YLS consists of a robotic control arm (KUKA), a working stage with four numerically controlled axes, a powder feeding system (GTV), and a nozzle head. A laser that is connected to the robotic system controls the processing. The nozzle is placed apart from the steel substrate by a certain amount. The admixed powders are fed coaxially using a commercial powder feeder mechanism (Figure 1b) with a flow balance to control the powder feed rate.

Through the use of a laser system, AlCuTi/Ti6Al4V was created. With various paper sizes, a standard procedure was used to characterize the materials for grinding and polishing. The samples were subjected to etching using the Nital reagent. After grinding and polishing, the specimens must be absolutely rinsed in distilled water and dried by air. All of the specimens were polished with diamond suspension, which gave them a mirror-like appearance. The specimens were then set up and kept in a desiccator. Prior to the specimens being characterized, the DLMD was reinforced with 99.98% pure aluminum, titanium, and copper powders with an average particle size of 90 microns. Aluminum, titanium, and copper reinforcements in various weight percentages were combined in a rotating plastic container using a Shimadzu measuring scale. Aluminum-copper-titanium mixes in the following weight percentages were used: aluminium-copper (4%)-titanium (7%) [900 W,

0.8 m/min], aluminium-copper (4%)-titanium (7%) [900 W, 1.0 m/min], aluminium-copper (4%)-titanium (7%) [1000 W, 0.8 m/min], aluminium-copper (4%)-titanium (7%) [1000 W, 1.0 m/min], aluminium-copper (7%)-titanium (5%) [900 W, 0.8 m/min], aluminium-copper (7%)-titanium (5%) [900 W, 1.0 m/min], aluminium-copper (7%)-titanium (5%) [1000 W, 0.8 m/min], and aluminium-copper (7%)-titanium (5%) [1000 W, 1.0 m/min], are three examples of alloys that contain titanium. The TLS firm, situated in Germany, produced reinforcement powders, which had a purity of 99.98% and were spherical in shape. Three types of reinforcement materials were used in this study: powders of copper, aluminum, and titanium. The powders were selected according to the unique characteristics they provide, which are utilized to create multifunctional systems and safe surfaces. TLS Technik GmbH & Co. Bitterfeld, Germany, provided the powders utilized in this project: Ti (99.98% purity, 90 μm average particle size), Al (99.98% purity, 90 μm average particle size), and Cu (99.98% purity, 90 μm average particle size). The tubular mixer (Figure 2) had a cylindrical container with reinforcement powders inside, and the speed and duration of the mixer were both adjusted to 72 rpm for 22 h. In order to achieve uniform mixes of the reinforcement powders, the mixer's speed and time were carefully chosen. The optical micrograph and SEM/EDS of the base alloy can be seen in Figures 3 and 4, while the composition and properties are seen in Tables 1 and 2.

Taguchi optimization technique was used for the process parameters. The technique lowers costs while simultaneously improving quality. The strategy is robust in that it improves the response while lessening its sensitivity to causes of variability. Process variables that are known and under control are referred to as signal factors, whereas process variables that are not under control are called noise factors. Depending on the intended response, Taguchi optimization uses one of three common signal-to-noise (S/N) ratios: nominal-is-best (NB), smaller-the-better (SB), or larger-the-better (LB). To optimize the laser power, scan velocity, and powder feed rate, as shown in Table 3, in terms of the composite coating's Vickers microhardness, tensile strength, and yield strength, this study used the L_8 Taguchi orthogonal array. The two levels at which each parameter was evaluated are displayed in Table 4. Table 4 displays the L_8 Taguchi orthogonal array according to the study's parameters, and Table 5 displays the appropriate input and output that were taken into account.

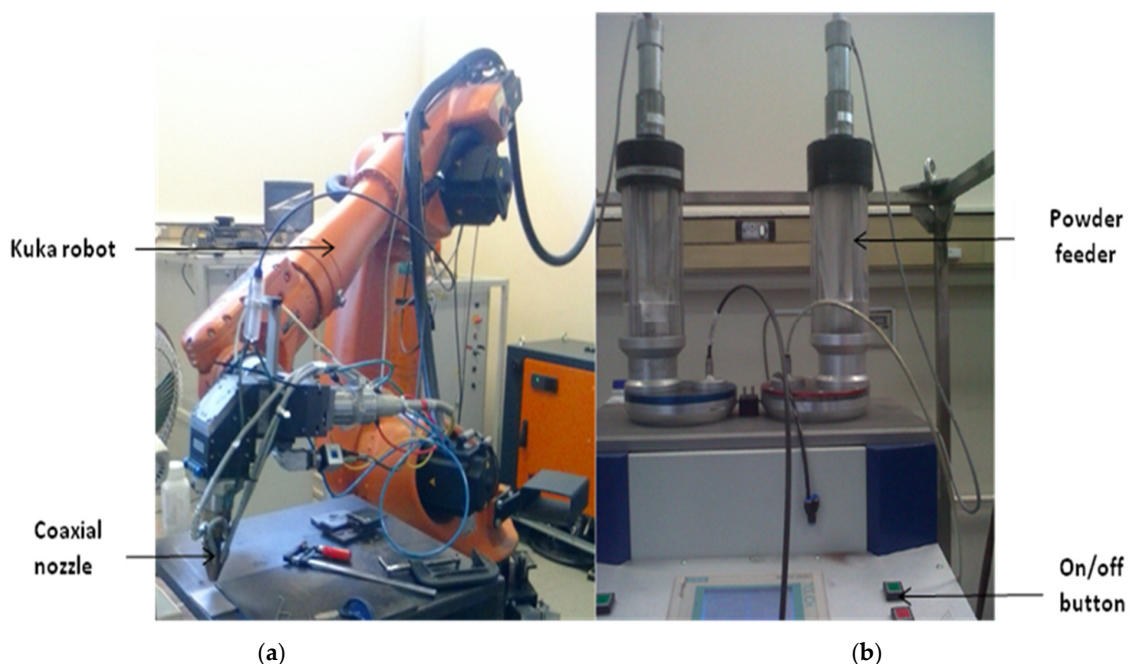


Figure 1. A 3000 W continuous-wave ytterbium laser system (YLS) connected to a KUKA robot (a) Ytterbium laser system (b) Powder feeders.



Figure 2. Turbula mixer.

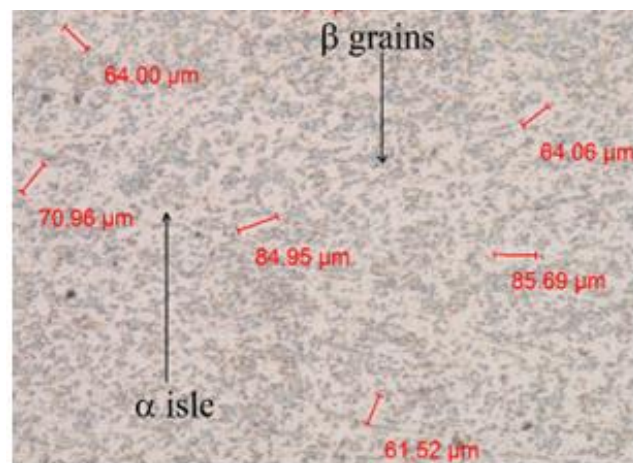


Figure 3. Optical micrograph of the substrate (Ti-6Al-4V) microstructure.

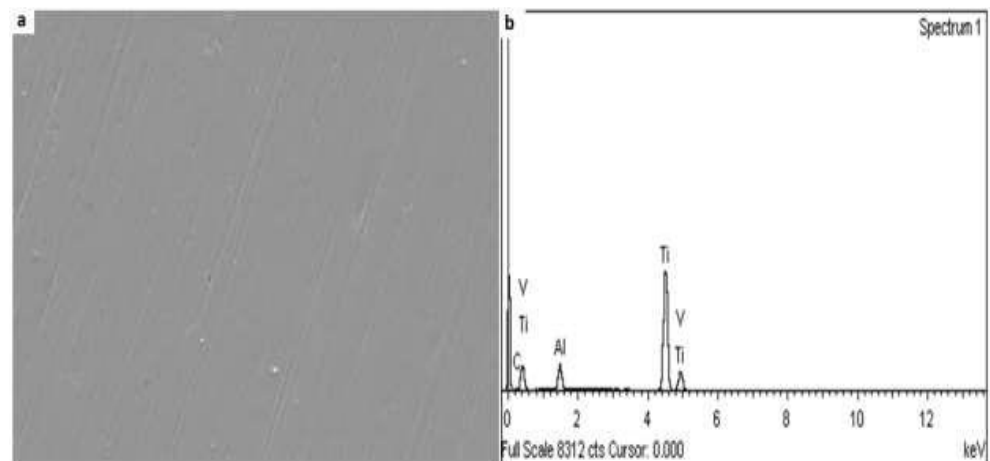


Figure 4. Microstructure of the substrate (Ti-6Al-4V) (a) Scanning electron microscopy (SEM) (b) Energy dispersive X-ray spectroscopy (EDX).

Table 2. Mechanical properties of the base metal.

Base Metal	Tensile Strength (MPa)	Yield Strength (MPa)	Vicker Hardness (HV)
Ti6Al4V	1170	1100	334

Table 3. Process parameters for laser deposition of Al-Cu-Ti/Ti-6Al-4V composite coatings.

Laser Power	900–1000 W
Laser scan speed	0.8–1.0 m/min
Laser beam diameter	2 mm
Powder flow rate	2.0–2.5 g/min
Shielding gas flow rate	Argon (2.0) L/min

Table 4. Experimental L₈ orthogonal matrix design.

Sample No	Laser Power (W)	Scan Velocity (m/min)	Powder Feed Rate (g/min)	Gas Flow Rate (L/min)
1	900	0.8	2.0	2.0
2	900	1.0	2.5	2.0
3	1000	0.8	2.5	2.0
4	1000	1.0	2.0	2.0
5	900	0.8	2.0	2.0
6	900	1.0	2.5	2.0
7	1000	0.8	2.5	2.0
8	1000	1.0	2.0	2.0

Table 5. Properties of AlCuTi/Ti6Al4V composite coatings.

Samples	Laser Power (W)	Scan Speed (m/min)	Average Hardness (HV _{0.1})	Tensile Strength (GPa)	Yield Strength (GPa)
Ti6Al4V alloy	-	-	345 ± 1.09	1.13	0.81
Ti6Al4V/Al-4Cu-7Ti	900	0.8	425 ± 3.16	1.39	1.00
Ti6Al4V/Al-4Cu-7Ti	900	1.0	644 ± 4.58	2.10	1.52
Ti6Al4V/Al-4Cu-7Ti	1000	0.8	346 ± 3.64	1.13	0.82
Ti6Al4V/Al-4Cu-7Ti	1000	1.0	396 ± 2.59	1.30	0.93
Ti6Al4V/Al-7Cu-5Ti	900	0.8	338 ± 1.59	1.10	0.80
Ti6Al4V/Al-7Cu-5Ti	900	1.0	1117 ± 2.37	3.64	2.64
Ti6Al4V/Al-7Cu-5Ti	1000	0.8	526 ± 1.02	1.72	1.24
Ti6Al4V/Al-7Cu-5Ti	1000	1.0	718 ± 3.14	2.34	1.69

The orthogonal design of the experimental technique properly followed the Design of Experiment (DOE). DOE was also used to optimize the parameters (Tables 3 and 4), which was necessary. As shown in Figure 1, the powder feed rate (the rate of flow of the powder in the nozzle) was set between 2.0–2.5 g/min, while the gas shield rate, which protects the flow of the powder via the nozzle, was set at 2.0 L/min. These parameters were tuned as shown in Table 3, and the laser power was set between 900 and 1000 W and the scan speed between 0.8 and 1.0 m/min. Since oxidation is bad news for DLMD, argon was used to protect the gas as it passed through the nozzle and touched the base metal's surface. Argon was chosen because it is less expensive than other gases. Each track's overlap during

DMLD was conducted at a percentage of 70%. After careful consideration, a space of 2 mm was decided upon between the nozzle tip and the metal's surface. The modified parameters, which in turn affect the microstructures, can be related to the improved qualities of the manufactured composite coatings, although only a few specimens had tiny pores visible. In order to obtain images of the microstructures, cross-sectional and surface views of the specimens were described. The optical images were captured using a Japanese-made Olympus microscope with the model number BX51M. The SEM pictures were obtained using scanning electron microscopy (SEM), also referred to as VEGA 3 TESCAN-XMAX. A Vickers microhardness tester with a diamond indenter was used to measure the alloyed samples' microhardness. At the interface, indentations were made with equal dimensions. Using a load of 100 gf and a 10 s dwell time, the microhardness of the samples was measured with a 50 μm gap between comparable indentations. Moreover, an X-ray diffractometer was used to obtain the XRD spectra.

3. Results and Discussion

3.1. Optical Microscopy (OM) and Scanning Electron Microscopy (SEM)

The heat differential caused the dendritic structures in the microstructures to form, as illustrated in Figures 5–10. The heat gradient influenced how much residual stress was present. These forces also had an impact on the improved microstructures' surface quality. Relative stresses may have a deleterious impact on composite coatings if they are too great. If not effectively controlled, these residual stresses could deform the composite coatings. The copper reinforcement employed used a stabilized phase known as the β -phase, which formed during the DMLD solidification phase and is particularly strong [30,31]. The propagation and initiation of the titanium phases are depicted in Figures 7 and 8. These phases were produced during the quick solidification by the chemical reaction of copper reinforcement and titanium alloy base metal in the melt pool. Dendritic grains produced by aluminum–copper structures were created by increasing the scan velocity, powder feed rate, and laser power [28,32]. According to Figures 7–10 the two phases produced can be categorized as eutectic phases and inter-dendritic intermetallics. The titanium alloy base metal's α (alpha) and β (beta) components helped to create the aforementioned phases. The titanium alloy base top surface and the laser nozzle tip had an impact on the phases that formed in the composite coatings. The creation of these phases depended on the molten pool's size and depth. The depth and extent of the molten pool were also influenced by the scanning speed and laser power. In additive manufacturing, the size of the melt pool and the creation of improved microstructures both have an impact on the mechanical properties.

First, the grains of the microstructures underwent a transition from columnar to equiaxial, and subsequently, tiny, large columnar grains became apparent in the microstructures (Figures 5 and 6). Enhancing the mechanical qualities requires careful consideration of how the melt pool is solidified. The thermal gradient and the rate of cooling have a significant impact on the size of the molten pool. As the laser travels from one point to another and interacts with the reinforcements, the temperature distribution changes. Grain propagation begins as soon as the laser beam interacts with the reinforcing powders. The rate of dilution in the molten pool between the titanium base alloy and the reinforcements must be thoroughly understood in the final microstructures of the composite coatings. Figures 7 and 8 show dendritic phases that were produced as a result of the copper and aluminum reacting in the melt pool.

The compositions used to create the microstructures are completely dependent on the heat gradient and solidification velocity. Because the laser nozzle rapidly cools as it moves from one point to another, the growth of the grains in the microstructure follows its motion. A 70% overlap was taken into account during the laser metal deposition process, and this serves as a type of heat treatment for the prior track. The equiaxed grains in the microstructures were produced by the heat treatment. Grain morphology changed as a result of variations in melt pool sizes brought on by varying rates of cooling and solidification.



Figure 5. Optical image of Al-4Cu-7Ti at 0.8 m/min and 900 W.

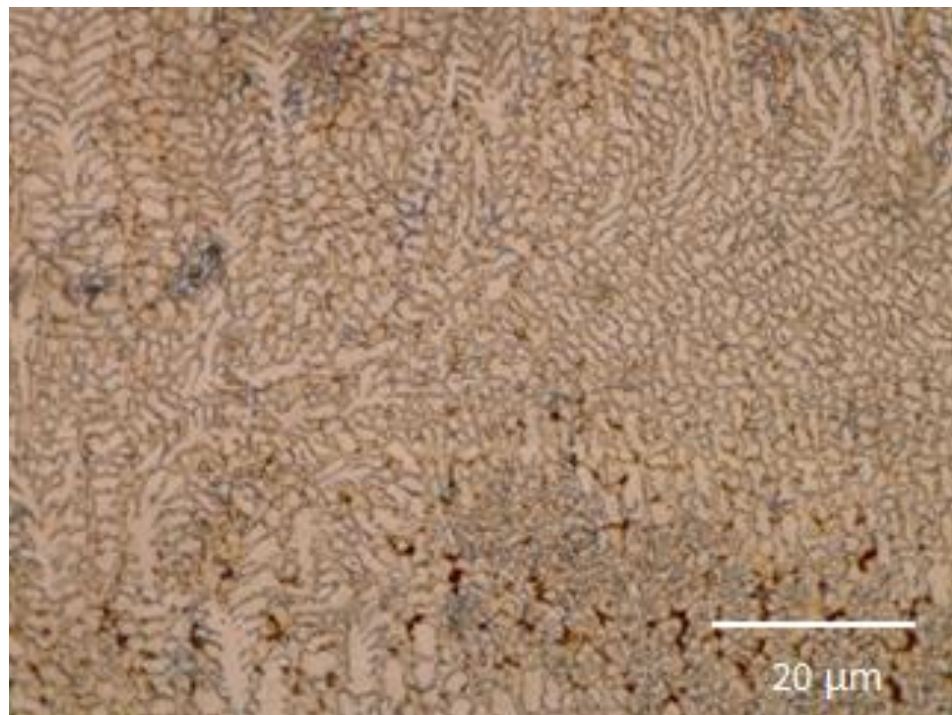


Figure 6. Optical image of Al-7Cu-5Ti at 1.0 m/min and 900 W.

This rate of cooling determines how quickly the beta phase in the titanium alloy base transitions to the alpha phase. The formation of a needle-like alpha phase (Figures 7b and 8b) occurred when the melt pool size was tiny. The combination of copper and aluminum has demonstrated good qualities. Together, they provide a powerful metallurgical link. In the microstructure, the development of composite coatings from the combination of copper and aluminum always results in two different phases: bright and dark occurs when the melt pool size is tiny. Because copper and aluminum are formed from the solid

solutions of the composite elements, their differences create a strong metallurgical bond. Columnar, equiaxed, and dendritic microstructures are the dark phases. While the light phase represents the primary titanium alloy, the dark phases can be seen in a variety of shapes and sizes. Copper as a reinforcement has been found to have beta-stabilizing properties by numerous research studies [33,34]. Because the titanium base alloy contains both alpha and beta phases, the fusion of copper reinforcement and the titanium alloy base metal resulted in the propagation of beta-titanium (β -Ti). As can be observed in Figures 9 and 10, titanium–aluminide (TiAl) was mostly formed due to the reinforcing of aluminum. The production of dark gray granules (alpha grain particles) indicates the presence of aluminum [35]. The beta-phase grains' brownish coloration, which shows the presence of copper, is apparent [36,37]. Dendritic structures began to propagate as the laser power and scan velocity were increased, demonstrating the presence of aluminum–copper (Al-Cu) in the microstructure [34,35].

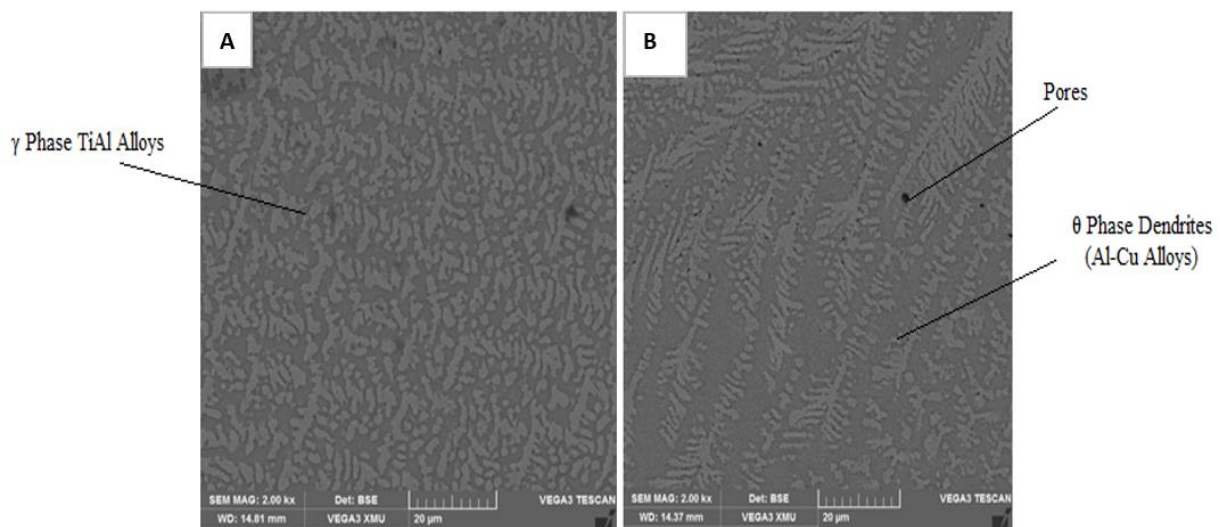


Figure 7. SEM image of composite coatings Ti-6Al-4V/Al-4Cu-7Ti (A) 1000 W, 0.8 m/min and (B) 1000 W, 1.0 m/min.

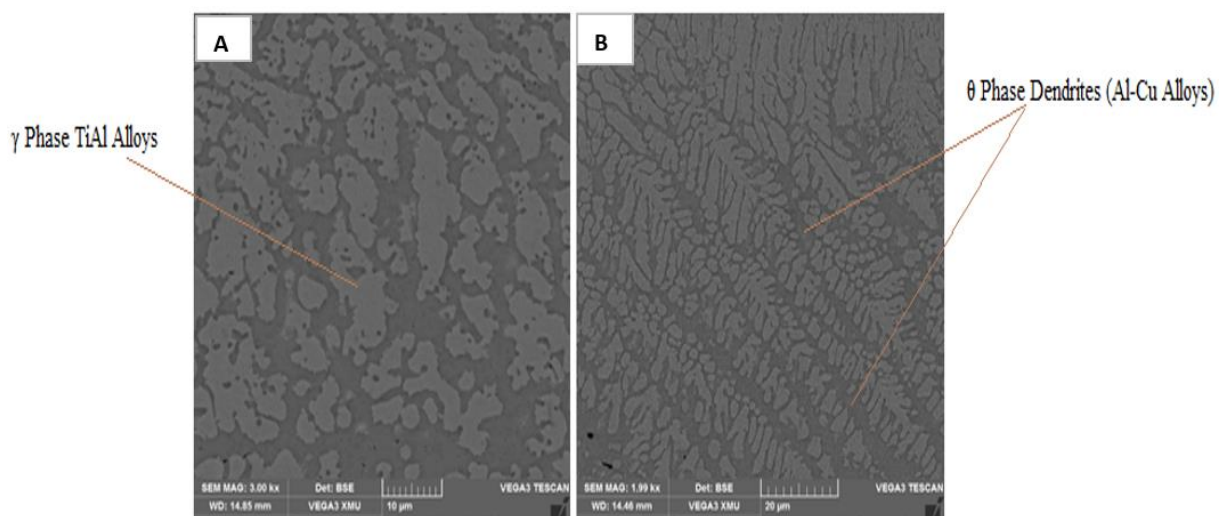


Figure 8. SEM image of composite coatings Ti-6Al-4V/Al-4Cu-7Ti (A) 900 W, 0.8 m/min and (B) 900 W, 1.0 m/min.

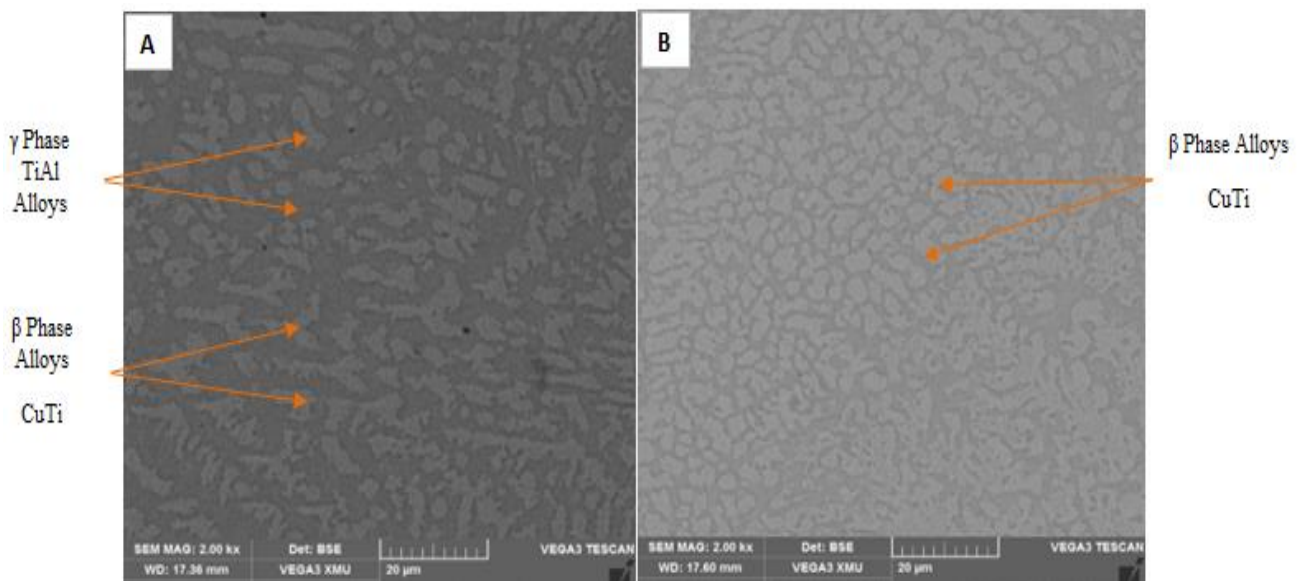


Figure 9. SEM image of composite coatings Ti-6Al-4V/Al-7Cu-5Ti (A) 900 W, 0.8 m/min and (B) 900 W, 1.0 m/min.

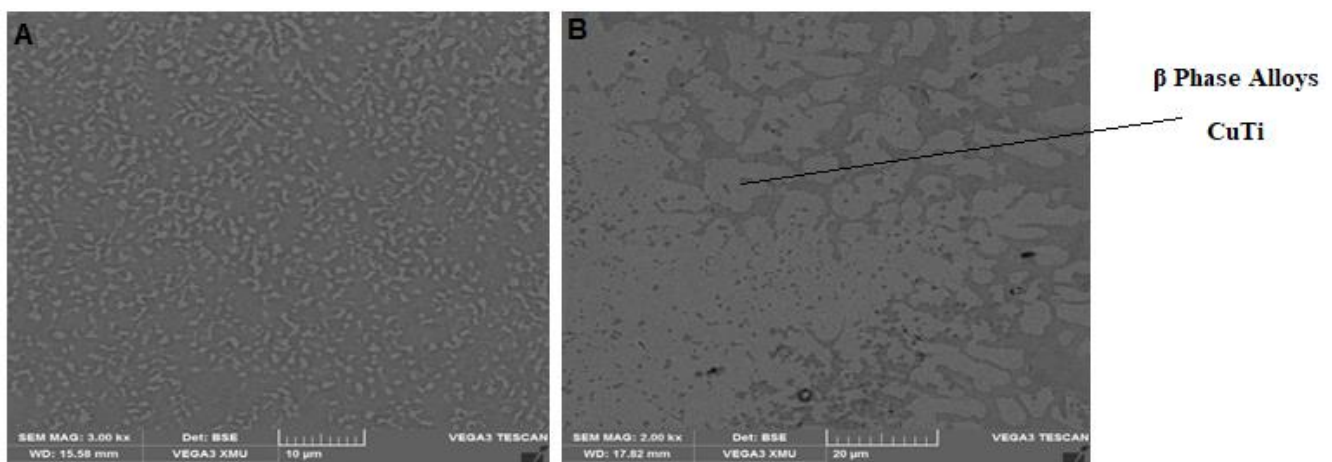


Figure 10. SEM image of composite coatings Ti-6Al-4V/Al-7Cu-5Ti (A) 1000 W, 0.8 m/min and (B) 1000 W, 1.0 m/min.

Low laser power results in weakly melted reinforcing powder particles, which leads to an unsatisfactory melting of high-pored quality coatings. The inability of the particles to form splats when the coatings are produced prevents them from conforming to the surface. Therefore, pores and cracks are created as a result of the splats' solidification.

Several unmelted and partially melted particles can also be found in the coatings that were applied using low laser power. It should be noted that an increase in laser power results in improvement, standardized distribution, and spheroidization, as well as an increase in the speed of the reinforcement particles that show a proper flow of molten liquid. The powder feed rate affects how many pores there would be in the coating. On the other side, the rate of deposition drives the rate of pores in the coatings. When compared to coatings created at 900 W and 1000 W, as shown in Figure 7, those created at 1000 W showed microscopic levels of apertures.

The increased degree of porosity at a higher powder feed rate is caused by the partially melted reinforcing powder that was deposited at the beam's nozzle tip. The initial laser power was insufficient to melt the reinforcement powder at a higher powder feed rate within a limited window of time, which resulted in partially melted reinforcement powder

in the molten pool and high porosity formation in the coating, as shown in Figure 7. Therefore, a method of preventing pores that might degrade the coatings' properties is to make thorough use of the optimized laser process. Combining the laser process parameters with a good powder feed rate is a viable technique for reducing the minute holes created in the microstructure. The distribution of the peak temperature in the molten pool depends on the distance from the Ti-6Al-4V alloy substrate. The powder feed rate, laser power, and scanning speed have a clear relationship.

3.2. X-ray Diffraction (XRD) Analysis

Binary intermetallic TiAl phases were found in both compositions of 4 and 7 weight percent copper, as shown in Figures 11 and 12.

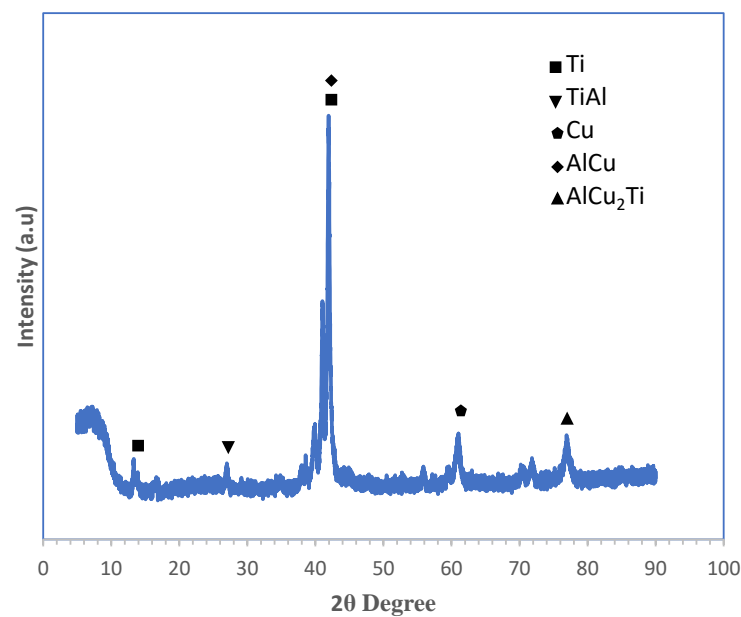


Figure 11. XRD spectrum of composite coatings Ti-6Al-4V / Al-4Cu-7Ti (1000 W, 1.0 m/min).

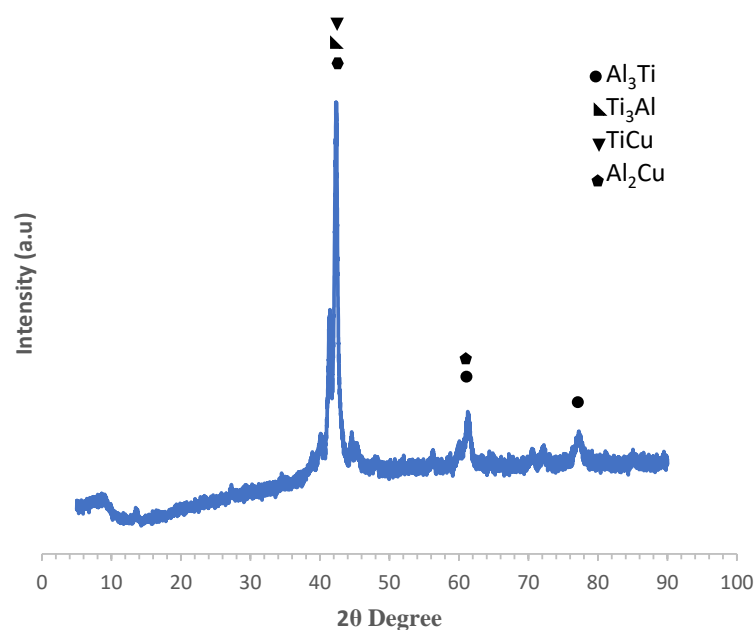


Figure 12. XRD spectrum of composite coatings Ti-6Al-4V / Al-7Cu-5Ti (900 W, 1.0 m/min).

Due to the various weight percentages of the copper and titanium reinforcements, variations in the composition of the diffraction peaks were noted. Due to titanium's highest weight percentage in the base metal (Ti6Al4V) and aluminum's highest weight percentage in the reinforcing powders, a peak of Ti, TiAl, and Al could be detected in Figure 11. Cu-Ti's intermetallic phases are created during solidification by a quick reaction between liquid and solid in the melt pool. These phases can assess the mechanical characteristics and microhardness of composite coatings. It has been documented in the literature that CuTi₂ is brittle and prone to cracking, but CuTi and TiCu are also known to be ductile. The phases that are created can have an impact on the composite coatings' mechanical characteristics.

The Ti6Al4V beta-phase change and the development of CuTi's intermetallic phases are both influenced by the laser's power intensity. The length of copper diffusion lengthens as laser power rises, increasing the thickness of CuTi's intermetallic phases. When the laser power intensity is decreased, the characteristics of CuTi can be improved [38–40]. Additionally, titanium–aluminide has been said to provide distinct strength at high temperatures, low density, and excellent oxidation resistance. Even at room temperature, the material is fragile due to its low fracture toughness, which has been documented in the literature. These outstanding qualities ultimately affect the characteristics of the composite coatings that are manufactured. Despite titanium aluminide's excellent properties, interlamellar spacing, lamella colony size, and alloying reinforcement addition made these properties possible. Reduced interlamellar spacing affects interlamellar strength at high temperatures [41,42].

3.3. Mechanical Properties of AlCuTi/Ti6Al4V Composite Coatings

The microhardness value of 643.6 HV_{1.0}, as shown in Table 5, with an increased scanning speed of 1.0 m/min, is responsible for the decreased laser power of 900 W. For composite coatings of Ti6Al4V and A4Cu7Ti, the next value of 424.5 HV_{1.0} at a scanning speed of 0.8 m/min still happened at 900 W of laser power. As shown in Figures 13 and 14, the same is true for Ti6Al4V/Al7Cu5Ti, which has a maximal hardness value of 1117.2 HV_{1.0} at 900 W of laser power and 1.0 m/min scanning speed.

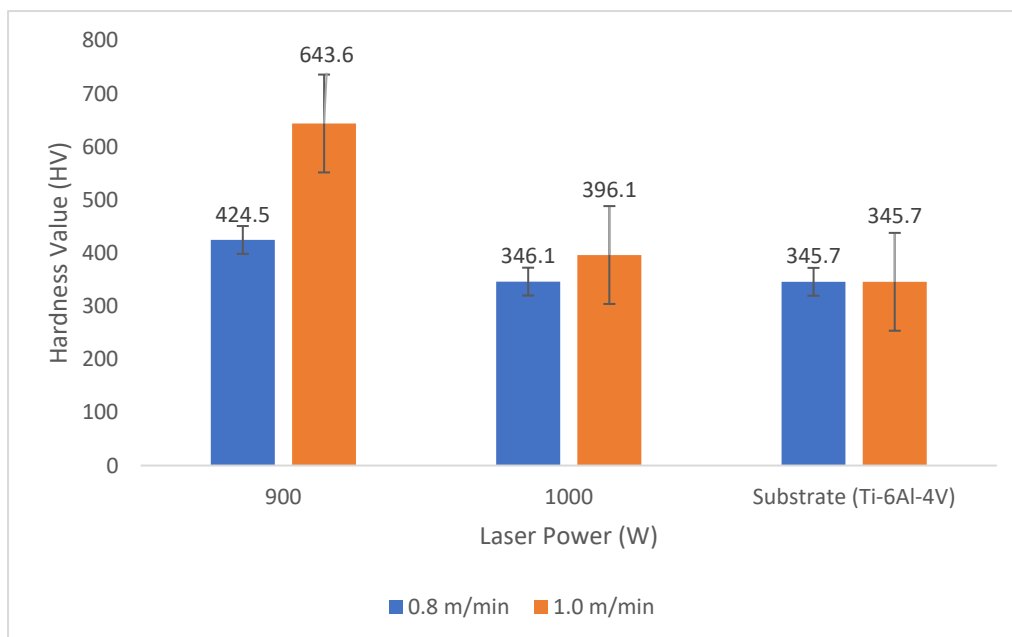


Figure 13. Microhardness graph of Ti-6Al-4V / Al-4Cu-7Ti composite coatings.

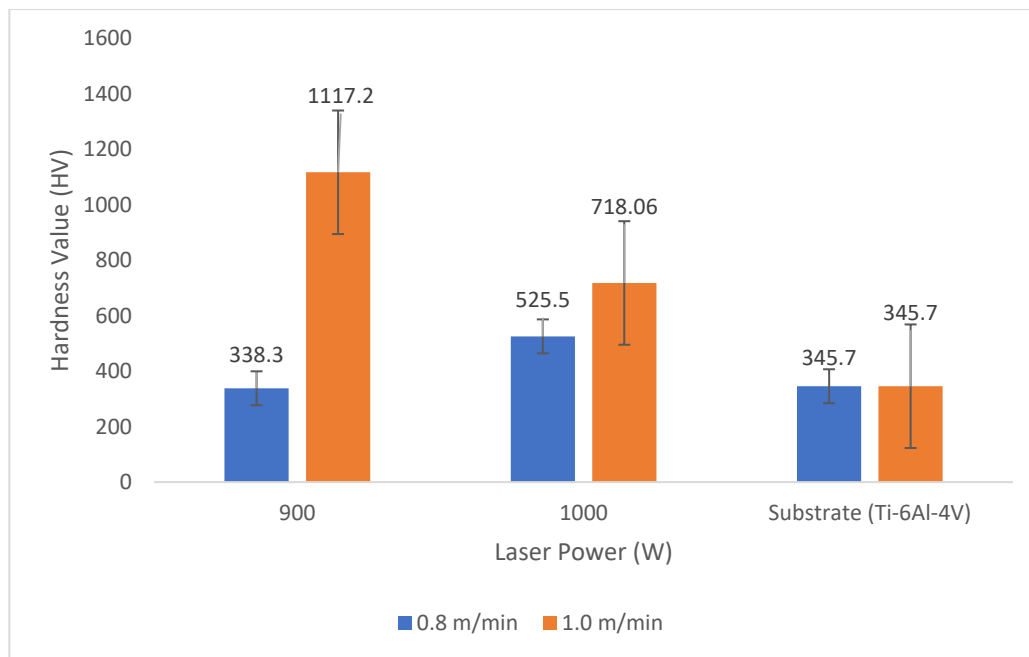


Figure 14. Microhardness graph of Ti-6Al-4V / Al-7Cu-5Ti composite coatings.

Several studies [43] say that the introduction of indentation testing led to the measurement of bulk hardness, which showed the mechanical properties of materials, like their tensile and yield strengths. Some researchers have proposed several equations to relate yield and tensile strengths to hardness indentation. These Equations (1) and (2) were used to calculate the mechanical characteristics of Al-Cu-Ti coatings [43]. Table 5 displays these numbers.

$$J = \left(\frac{G}{2.9}\right)\left(\frac{k}{0.217}\right)^k \quad (1)$$

$$L = \left(\frac{G}{3}\right)(0.1)^k \quad (2)$$

G stands for the Vickers hardness values, while k represents the strain hardening coefficient, which has a value of 0.15 [43]. J stands for tensile strength, and L for yield strength. Table 5 shows improvements in the tensile and yield strengths when compared to titanium alloy, the basis metal. Certain scholars also indicated other linear Equations (3) and (4), which relate Vickers hardness indentations to both the yield and ultimate tensile strengths [44].

$$J = -99.8 + 3.734G \quad (3)$$

$$L = -90.7 + 2.876G \quad (4)$$

No other variables are required to calculate the tensile and yield strengths of materials except the Vickers hardness values. Tensile and yield strengths are affected by copper and titanium content up to maximum values of 3.64 and 2.64 GPa, respectively, at 7 percent copper and 5 percent titanium. The findings demonstrate that the coatings' yield and tensile strengths are improved in comparison to those of the substrate (Ti-6Al-4V alloy).

The yield strength and tensile strength of the ternary coatings, two mechanical qualities, improved. The coatings on samples 1, 2, 4, 6, 7, and 8 showed tensile strengths of 1.39 GPa, 2.10 GPa, 1.30 GPa, 3.64 GPa, 1.72 GPa, and 2.34 GPa, respectively. Tensile strengths of laser-clad ternary coatings are improved by 23%, 46.2%, 13.1%, 70%, 34.3%, and 51.7% when compared to titanium alloy substrates. The yield strengths of the coatings on samples 1, 2, 4, 6, 7, and 8 were 1.00 GPa, 1.52 GPa, 0.93 GPa, 2.64 GPa, 1.24 GPa, and

1.69 GPa, respectively. The yield strengths of laser-clad ternary coatings are improved by 19%, 46.7%, 12.9%, 69.3%, 34.7%, and 52.1% when compared to the titanium alloy substrate.

As shown in Table 5, refined grains have a considerable impact on the hardness ratings and microstructures of the coatings. The combined strengthening effects induced by the presence of these hard intermetallic phases inside the coatings are what give laser-clad ternary coatings their enhanced mechanical properties. This was a result of the experimental work's optimized process parameters. The mechanical properties of the copper–titanium-added aluminum matrix are affected. By carefully regulating the ratio and distribution of the components of a composite, as well as the processing conditions [45], these can be further improved by the inclusion of a modest weight percent of copper and titanium into the matrix. According to the findings, Table 5 clearly demonstrates the impact of weight percentages of copper and titanium and carefully chosen processing conditions on the laser-clad ternary coatings' tensile and yield strengths.

The presence of titanium–aluminide phases, detected in the XRD, contributed to the increased hardness, tensile strength, and yield strength because the hardness values are also influenced by the excellent properties of titanium aluminide. The increased mechanical properties of the composite coatings are related to the strength of titanium aluminide phases generated at high temperatures during fast solidification in the melt pool. The hardest composite coatings measured a microhardness of 1117.2 HV_{1.0}, which is comparable to a 69.1% increase in hardness over the base alloy.

3.4. Geometrical Characteristics

Figure 15a,b show that the height of the heat-affected zone (HAZ), the height of the deposit (coatings) on the base alloy, and the changes in the laser power used for the LMD operation are all geometric parameters that are closely related to each other. As demonstrated in Figure 16a, this interaction also has an impact on deposit width. Composites with 900 W laser energy input had narrower deposits, but composites with a 1000 W laser power increase had wider deposits. The clad's height and width [46] demonstrate that the 900 W laser power was adequate to produce composites with dense geometric features. The clad becomes thinner and slenderer as a result of the increased energy of the LMD operation [46]. The relationship between the rate of dilution and laser power is seen in Figure 16b. The composites' rate of dilution shows that when the laser power of the LMD operation is increased, so is the rate at which the coating materials diffuse into the base alloy's structural matrix and mix the metallurgical properties of the components. The composite with the highest rate of dilution is Ti6Al4V/Al7Cu5Ti. This indicates that the fast diffusion of the coating components into the base alloy (substrate) is made possible by raising the copper content of the base alloy's structural matrix [47].

The analysis of the height features in relation to the variations in scanning speed for the deposit height and HAZ height is shown in Figure 17. The geometrical height features of the deposited clad diminish with the increasing scanning speed of the LMD operation, as indicated by the graphed results shown in Figure 17a,b. This occurs as a result of the wide range of powder materials that are ready to react with the laser and form dense deposits in the clad. More coating material was deposited per unit length of base alloy when the scanning speed was slower. This suggests that the coating materials had more time to interact with the laser and fuse with it. Because there was not enough time for the coating materials to interact with the laser and fuse with the base alloy, less dense composites were generated as a result of the higher scanning speed of the LMD operation. Further support for these results comes from the graph showing the deposit width as a function of scanning speed. The rate of dilution of the coating materials inside the base alloy's structural matrix increases as the scanning speed of the LMD operation increases, as seen by the graph depicting the rate of dilution as a function of scanning speed (Figure 18) [48]. This shows that more coating components work in concert with the underlying alloy to produce composites with a higher scanning speed. The LMD operation's deposit width reduced (Figure 19) when the scanning speed increased and increased when the scanning

speed decreased, owing to the additional time given to the coating materials to interact with the laser and fuse with the base alloy [40,41]. This implies that the base alloy and coating components mix effectively beneath the surface of the deposited clad [49,50].

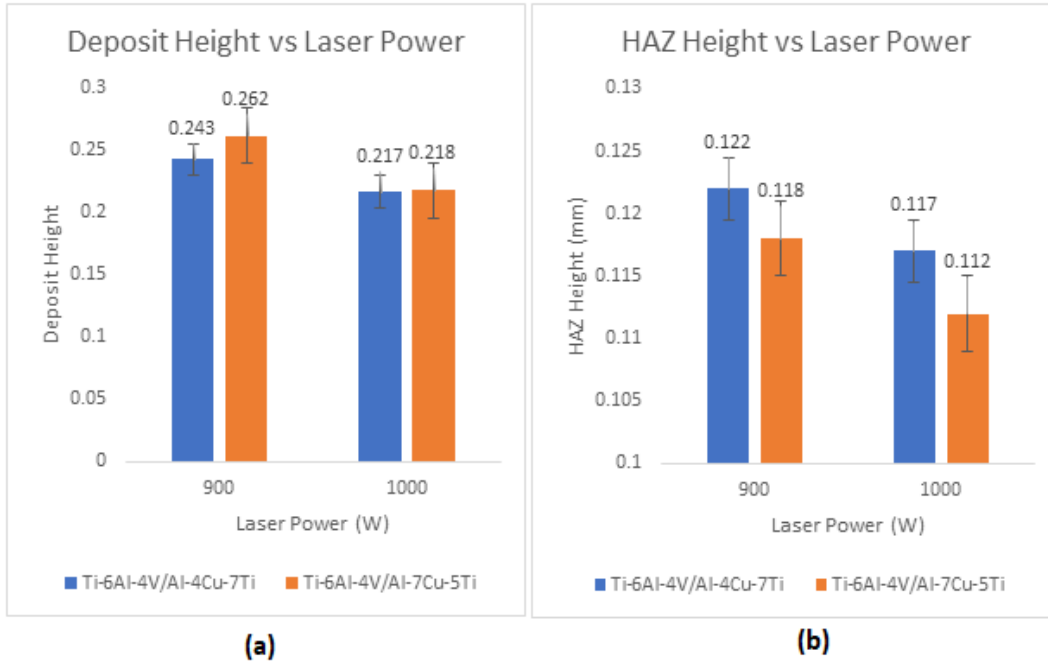


Figure 15. Graph of composite coatings geometrical heights and HAZ (a) deposit height against laser power and (b) HAZ height against laser power.

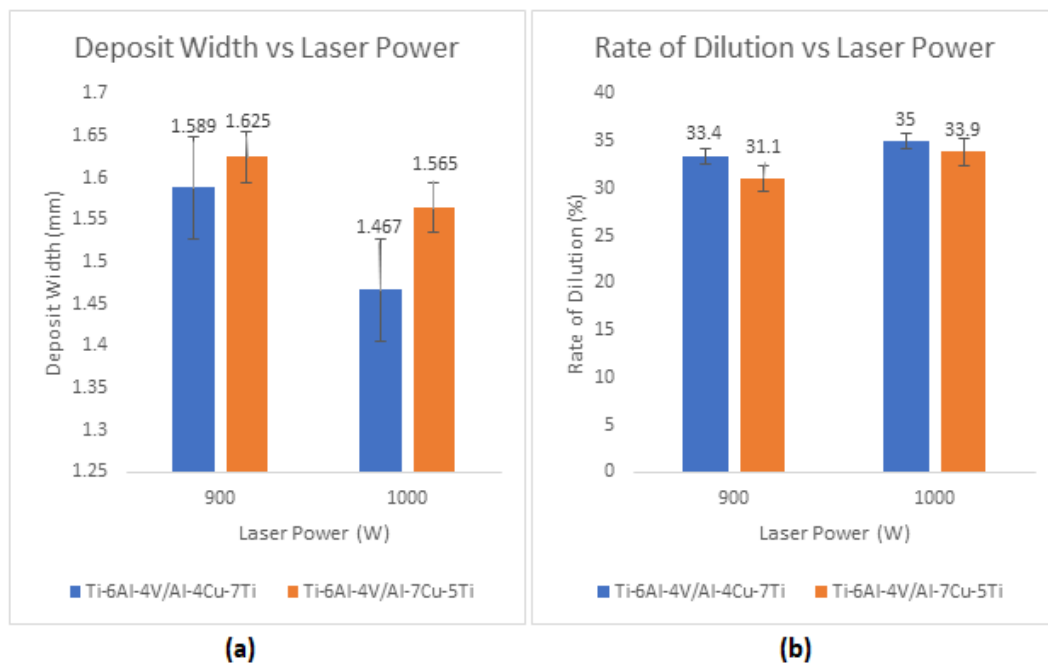


Figure 16. Graph of composite coatings geometrical width and dilution (a) deposit width against laser power and (b) rate of dilution against laser power.

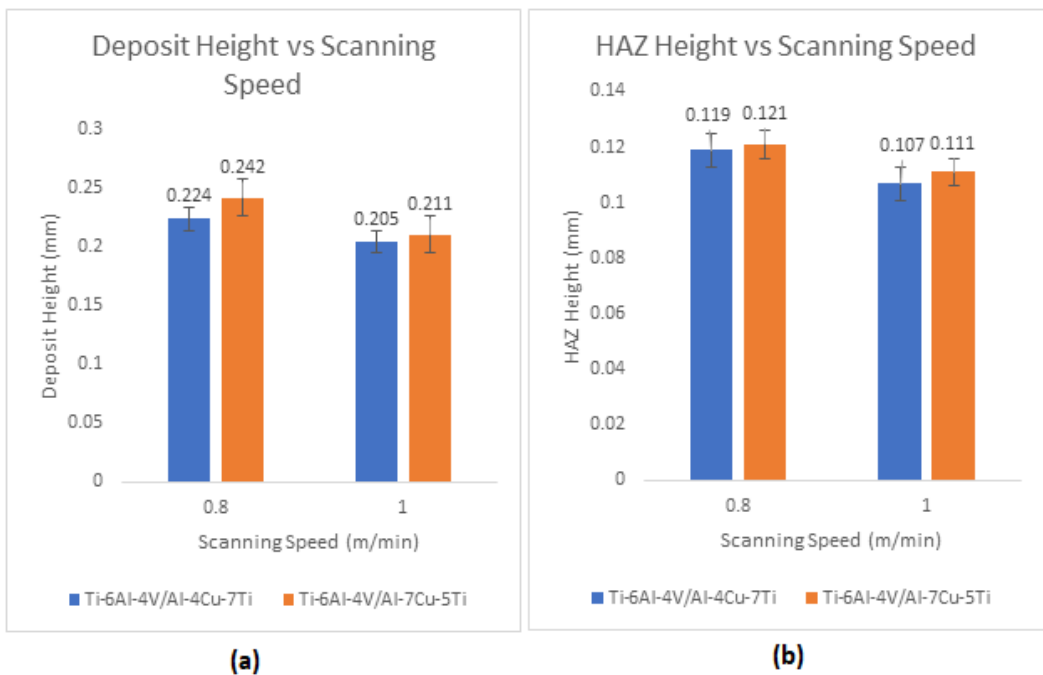


Figure 17. Graph of composite coatings geometrical heights and HAZ (a) deposit height against scanning speed and (b) HAZ height against scanning speed.

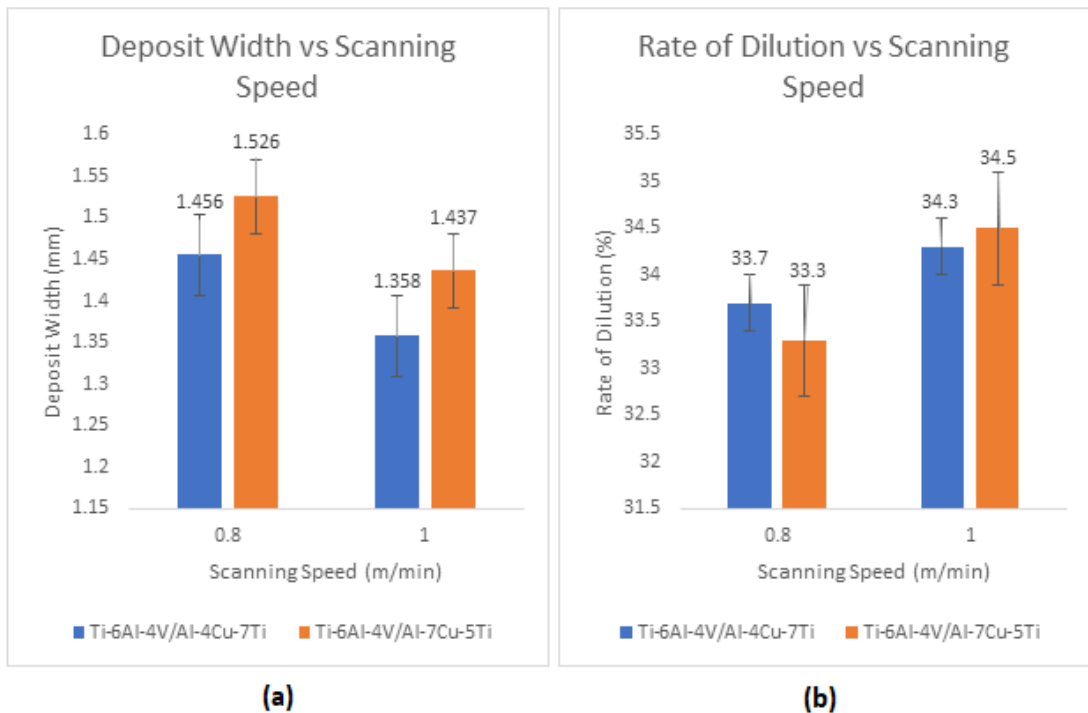


Figure 18. Graph of composite coatings geometrical width and dilution (a) deposit width against scanning speed and (b) rate of dilution against scanning speed.

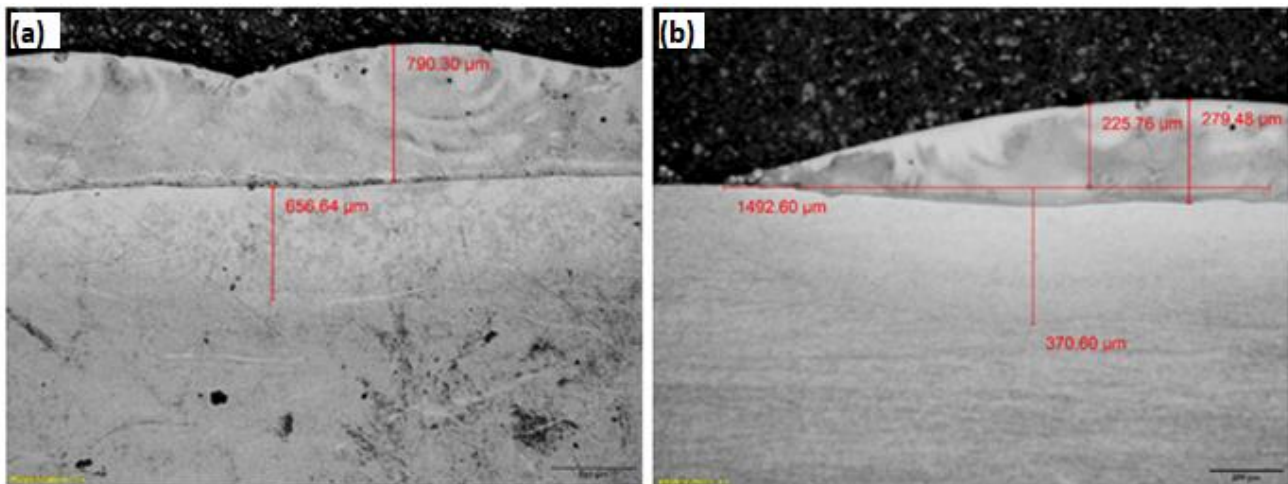


Figure 19. Optical micrographs cross-sections of composite coatings Ti-6Al-4V/Al-7Cu-5Ti (a) 900 W, 0.8 m/min and (b) 900 W, 1.0 m/min.

4. Conclusions

- Using the laser surface modification approach, new advanced metallic ternary coatings with improved characteristics were successfully fabricated.
- By optimizing the laser processing parameters and carefully choosing reinforcement material fractions, high residual stresses and the formation of cracks were kept to a minimum. This improved the quality of the coatings, the surface adhesion of the substrate and reinforcement materials, the evolution of the microstructure, and the mechanical properties as a whole.
- The optimal scan speed, laser power, and reinforcement (powder) feed rate led to dendritic grain propagation, which led to the formation of aluminum–copper structures. The employed reinforcing power, such as copper, stabilized the beta particles in the microstructures that were created. Furthermore, AlCuTi/Ti6Al4V composite coatings have been created using the laser cladding process for long-term aerospace applications.
- The strength of the laser beam affects the formation of CuTi intermetallic phases and the beta-phase change of Ti6Al4V. The length of copper’s diffusion rises with increasing laser power, which results in an increase in the thickness of the CuTi intermetallic phases. By lowering the laser light intensity, CuTi’s characteristics can be improved.
- The highest microhardness value of 1117.2 HV1.0, in comparison to the base alloy, corresponds to a 69.1% increase in the hardness of the composite coatings. When the process parameters were optimized, dendritic phases were formed in the microstructures. These phases were linked to the hardness improvement. Due to the fact that titanium aluminide’s superior qualities also affect the hardness ratings, this improved hardness attribute of the composite coatings is related to the strength of titanium aluminide phases generated at elevated temperatures during rapid solidification in the melt pool.
- Two mechanical properties of the ternary coatings (yield strength and tensile strength) were enhanced. The tensile strengths of laser-clad ternary coatings were 23%, 46.2%, 13.1%, 70%, 34.3%, and 51.7% better than those of titanium alloy substrates. Comparing the yield strengths of the laser-clad ternary coatings to the titanium alloy substrate, the improvements were 19%, 46.7%, 12.9%, 69.3%, 34.7%, and 52.1%.

Author Contributions: O.S.F.—writing—review, editing, methodology, conceptualization, original draft preparation, data curation, validation, data analysis, visualization. T.-C.J.—writing—review, editing, visualization, data analysis, data curation. All authors have read and agreed to the published version of the manuscript.

Funding: This research received no external funding.

Data Availability Statement: Not applicable.

Acknowledgments: The Laser System used for the experimental work was provided by CSIR National Laser Center, South Africa. This is highly appreciated.

Conflicts of Interest: The authors declare no conflict of interest.

References

1. Dursun, T.; Soutis, C. Recent Developments in Advanced Aircraft Aluminium Alloys Review Article. *Mater. Des.* **2014**, *56*, 862–871. [[CrossRef](#)]
2. Shao, M.; Wang, W.; Yang, H.; Zhang, X.; He, X. Preparation of Wear-Resistant Coating on Ti6Al4V Alloy by Cold Spraying and Plasma Electrolytic Oxidation. *Coatings* **2021**, *11*, 1288. [[CrossRef](#)]
3. Lim, J.M.; So, Y.S.; Kim, J.G. Microstructure and Corrosion Behavior of Laser-Welded Al–Mn–Zr Alloy for Heat Exchanger. *Materials* **2023**, *16*, 6009. [[CrossRef](#)] [[PubMed](#)]
4. Kwok, C.T.; Cheng, F.T.; Man, H.C. Cavitation Erosion and Corrosion Behaviour of Laser-Aluminized Mild Steel. *Surf. Coat. Technol.* **2006**, *200*, 3544–3552. [[CrossRef](#)]
5. Dobrzanski, L.A.; Piec, M.; Bonek, M.; Jonda, E.; Klimpel, A. Mechanical and Tribological Properties of Laser Alloyed Surface Coatings. *J. Achiev. Mater. Manuf. Eng.* **2007**, *20*, 235–238.
6. Wei, L.; Huijun, Y.; Chuanzhong, C.; Diangang, W.; Fei, W. Microstructures of Hard Coatings Deposited on Titanium Alloys by Laser Alloying Technique. *J. Surf. Rev. Lett.* **2013**, *20*, 1350007.
7. Fagnolo, J.B.; Rodrigues, A.V.; Lima, M.S.F.; Amigo, V.; Caram, R. A Novel Proposal to Manipulate the Properties of Titanium Parts by Laser Alloying. *Scr. Mater.* **2013**, *68*, 471–474. [[CrossRef](#)]
8. Pham, N.T.H.; Nguyen, V.T. Wear Properties of TiC-Reinforced Co50 Composite Coatings from Room Temperature to High Temperature. *Adv. Mater. Sci. Eng.* **2020**, *2020*, 6849081. [[CrossRef](#)]
9. Fatoba, O.S.; Jen, T.C.; Akinlabi, E.T. Experimental Study on Microstructural Evolution, Mechanical Property, and Corrosion Behaviour of Laser Additive Manufactured (LAM) Titanium Alloy Grade 5. *Int. J. Adv. Manuf. Technol.* **2021**, *114*, 655–669. [[CrossRef](#)]
10. Poulon-Quintin, A.; Watanabe, I.; Watanabe, E.; Bertrand, C. Mechanical and Microstructural Properties of Surface Treated Cast Titanium with Nd: Yag Laser. *Dent. Mater.* **2012**, *24*, 2769–2783.
11. Yakovlev, A.; Bertrand, P.H.; Smurov, I. Laser Cladding of Wear Resistant Metal Matrix Composite Coatings. *Thin Solid Films* **2004**, *453*, 133–138. [[CrossRef](#)]
12. Berger, R. *Additive Manufacturing: A Game Changer for the Manufacturing Industry*; Roland Berger Strategy Consultants GmbH: Munich, Germany, 2013; Volume 1 (5.1).
13. Coykendall, J.; Holdowsky, J.; Cotteleer, M.; Mahto, M. 3D opportunity in aerospace and defense: Additive manufacturing takes flight. *Deloitte Insights* **2014**, *2*, 1.
14. Debroy, T.; Wei, H.; Zuback, J.; Mukherjee, T.; Elmer, J.; Milewski, J.; Beese, A.M.; Wilson-Heid, A.; De, A.; Zhang, W. Additive manufacturing of metallic components—process, structure and properties. *Prog. Mater. Sci.* **2018**, *92*, 112–224. [[CrossRef](#)]
15. Esmaeilian, B.; Behdad, S.; Wang, B. The evolution and future of manufacturing: A review. *J. Manuf. Syst.* **2016**, *39*, 79–100. [[CrossRef](#)]
16. Borish, M.; Gibson, B.T.; Adkins, C.; Mhatre, P. Automated Process Planning for Embossing and Functionally Grading Materials via Site-Specific Control in Large-Format Metal-Based Additive Manufacturing. *Materials* **2022**, *15*, 4152. [[CrossRef](#)] [[PubMed](#)]
17. Eckert, C.; Wynn, D.C.; Maier, J.F.; Albers, A.; Bursac, N.; Chen, H.L.X.; Clarkson, P.J.; Gericke, K.; Gladysz, B.; Shapiro, D. On the integration of product and process models in engineering design. *Des. Sci.* **2017**, *3*, e3. [[CrossRef](#)]
18. Mugwagwa, L.; Dimitrov, D.; Matope, S.; Yadroitsev, I. Influence of process parameters on residual stress related distortions in selective laser melting. *Procedia Manuf.* **2018**, *21*, 92–99. [[CrossRef](#)]
19. Wang, C.; Loh, Y.M.; Cheung, C.F.; Liang, X.; Zhang, Z.; Ho, L.T. Post processing of additively manufactured 316L stainless steel by multi-jet polishing method. *J. Mater. Res. Technol.* **2023**, *23*, 530–550. [[CrossRef](#)]
20. Liu, S.S.; Wang, X.H.; Zhang, M.; Zhao, G.L. Fabrication of CNTs–TiC–Ti2(Ni,Al) Ni3Ti reinforced Ti-based composite coating by laser alloying processing. *J. Mater. Res. Technol.* **2019**, *8*, 5930–5940. [[CrossRef](#)]
21. Phutela, C.; Aboulkhair, N.T.; Tuck, C.J.; Ashcroft, I. The Effects of Feature Sizes in Selectively Laser Melted Ti-6Al-4V Parts on the Validity of Optimized Process Parameters. *Materials* **2020**, *13*, 117. [[CrossRef](#)]
22. Fiolek, A.; Zimowski, S.; Kopia, A. Effect of Low-Friction Composite Polymer Coatings Fabricated by Electrophoretic Deposition and Heat Treatment on the Ti-6Al-4V Titanium Alloy’s Tribological Properties. *Metall. Mater. Trans. A* **2020**, *51*, 4786–4798. [[CrossRef](#)]
23. Gharehbaghi, R.; Fatoba, O.S.; Akinlabi, E.T. Influence of Scanning Speed on the Microstructure of Deposited Al-Cu-Fe Coatings on a Titanium Alloy Substrate by Laser Metal Deposition Process. In Proceedings of the 2018 IEEE 9th International Conference on Mechanical and Intelligent Manufacturing Technologies (ICMIMT 2018), Cape Town, South Africa, 10–13 February 2018; pp. 44–49. [[CrossRef](#)]

24. Fatoba, O.S.; Adesina OSPopoola, A.P.I. Evaluation of microstructure, microhardness, and electrochemical properties of laser-deposited Ti-Co coatings on Ti-6Al-4V Alloy. *Int. J. Adv. Manuf. Technol.* **2018**, *97*, 2341–2350. [[CrossRef](#)]
25. Yadav, S. A Review on Enhancement of Wear Resistance. *IOP Conf. Ser. Mater. Sci. Eng.* **2018**, *455*, 012120. [[CrossRef](#)]
26. Wang, X.; Yanpei, L.; Junjian, H.; Wenbin, H.; Kun, L.; She, Z. Preparation and Properties of Core-Shell Structure/Ni60 Coating. *Shock. Vib.* **2021**, *2021*, 2557539. [[CrossRef](#)]
27. Huang, C.; Li, H.; Li, D.; Lin, S. The performance of titanium composite coatings obtained through thermal spraying and microarc oxidation. *Compos. Adv. Mater.* **2021**, *30*. [[CrossRef](#)]
28. Yang, C.; Zhao, H.; Qu, S.; Li, X.; Li, Y. New development of Ti-based alloys for biomedical applications. *Materials* **2014**, *7*, 1709–1800.
29. Gharehbaghi, R.; Fatoba, O.S.; Akinlabi, E.T. Experimental Investigation of Laser Metal Deposited Icosahedral Al-Cu-Fe Coatings on Grade Five Titanium Alloy. In Proceedings of the 2018 IEEE 9th International Conference on Mechanical and Intelligent Manufacturing Technologies (ICMIMT 2018), Cape town, South Africa, 10-13 February 2018; pp. 31–36. [[CrossRef](#)]
30. Zhong, C.; Liu, J.; Zhao, T.; Schopphoven, T.; Fu, J.; Gasser, A.; Schleifenbaum, J.H. Laser Metal Deposition of Ti6Al4V—A Brief Review. *Appl. Sci.* **2020**, *10*, 764. [[CrossRef](#)]
31. Li, T.; Wang, Z.; Hu, S.; Yang, Z.; Wang, Y. Hot cracking during the fabrication of Inconel 625/stainless steel 308 L functionally graded material by dual-wire arc additive manufacturing. *J. Manuf. Process.* **2022**, *82*, 461–473. [[CrossRef](#)]
32. Tapoglou, N.; Clulow, J.; Curtis, D. Increased shielding of a direct energy deposition process to enable deposition of reactive materials; an investigation into deposition of 15-5 PH stainless steel, Inconel 718 and Ti-6Al-4V. *CIRP J. Manuf. Sci. Technol.* **2022**, *36*, 227–235. [[CrossRef](#)]
33. Lee, H.J.; Narayana, P.L.; Kim, J.H.; Park, C.H.; Hong, J.K.; Yeom, J.T.; Lee, T.; Lee, S.W. Effect of interlayer cooling on the microstructure and mechanical properties of titanium alloys fabricated using directed energy deposition. *J. Alloys Compd.* **2023**, *953*, 170202. [[CrossRef](#)]
34. Narayana, P.L.; Lee, S.; Choi, S.W.; Li, C.L.; Park, C.H.; Yeom, J.T.; Reddy, N.S.; Hong, J.K. Microstructural response of β -stabilized Ti-6Al-4V manufactured by direct energy deposition. *J. Alloys Compd.* **2019**, *811*, 152021. [[CrossRef](#)]
35. Chlupová, A.; Heczko, M.; Obrtlík, K.; Dlouhý, A.; Kruml, T. Effect of heat-treatment on the microstructure and fatigue properties of lamellar γ -TiAl alloyed with Nb, Mo and/or C. *Mater. Sci. Eng. A* **2020**, *786*, 139427. [[CrossRef](#)]
36. Tan, X.P.; Chandra, S.; Kok, Y.; Tor, S.B.; Seet, G.; Loh, N.H.; Liu, E. Revealing competitive columnar grain growth behavior and periodic microstructural banding in additively manufactured Ti-6Al-4V parts by selective electron beam melting. *Materialia* **2019**, *7*, 100365. [[CrossRef](#)]
37. Huang, H.; Ding, H.; Xu, X. The microstructure and mechanical property of TiAl alloy containing Beta Stabilizer. *Procedia Manuf.* **2019**, *37*, 73–79. [[CrossRef](#)]
38. Zhu, Y.Y.; Tang, H.B.; Li, Z.; Xu, C.; He, B. Solidification behavior and grain morphology of laser additive manufacturing titanium alloys. *J. Alloys Compd.* **2019**, *777*, 712–716. [[CrossRef](#)]
39. Yang, Y.; Liu, Y.J.; Chen, J.; Wang, H.L.; Zhang, Z.Q.; Lu, Y.J.; Wu, S.Q.; Lin, J.X. Crystallographic features of α variants and β phase for Ti-6Al-4V alloy fabricated by selective laser melting. *Mater. Sci. Eng. A* **2017**, *707*, 548–558. [[CrossRef](#)]
40. Obiegbu, M.C.; Fatoba, O.S.; Akinlabi, E.T.; Akinlabi, S.A. Experimental Study on Characteristics of Laser Metal Deposited Al-Si-Sn-Cu/Ti-6Al-4V composite coatings. *Mater. Express Res.* **2019**, *6*, 1–11. [[CrossRef](#)]
41. Li, F.C.; Liu, T.; Zhang, J.Y.; Shuang, S.; Wang, Q.; Wang, A.D.; Wang, J.G.; Yang, Y. Amorphous–nanocrystalline alloys: Fabrication, properties, and applications. *Mater. Today Adv.* **2019**, *4*, 100027. [[CrossRef](#)]
42. Wang, T.; Li, B.; Wang, Z.; Nie, Z. A microstructure with improved thermal stability and creep resistance in a novel near-alpha titanium alloy. *Mater. Sci. Eng. A* **2018**, *731*, 12–20. [[CrossRef](#)]
43. Cahoon, J.R.; Broughton, W.H.; Kutzak, A.R. The determination of yield strength from hardness measurements. *Metall. Trans.* **1971**, *2*, 1979–1983. [[CrossRef](#)]
44. Chenna, K.S.; Kumar, G.N.; JhaAbhay, K.; Bhanu, P. On the prediction of strength from hardness for copper alloys. *J. Mater.* **2013**, *2013*, 352578. [[CrossRef](#)]
45. Mishra, A.; Paul, A.R.; Mukherjee, M.; Singh, R.K.; Sharma, A.K. Evaluation of Cu-Ti dissimilar interface characteristics for wire arc additive manufacturing process. *Rapid Prototyp. J.* **2023**, *29*, 366–377. [[CrossRef](#)]
46. Ridolfi, M.R.; Folgarait, P.; Battaglia, V.; Vela, T.; Corapi, D.; Di Schino, A. Development and Calibration of a CFD Based Model of the Bed Fusion SLM Additive Manufacturing Process aimed at Optimising Laser Parameters. *Procedia Struct. Integr.* **2019**, *34*, 370–380. [[CrossRef](#)]
47. Yao, J.; Suo, T.; Zhang, S.; Zhao, F.; Wang, H.; Liu, J.; Chen, Y.; Li, Y. Influence of heat-treatment on the dynamic behavior of 3D laser-deposited Ti-6Al-4V alloy. *Mater. Sci. Eng. A* **2016**, *677*, 153–162. [[CrossRef](#)]
48. Lervåg, M.; Sørensen, C.; Robertstad, A.; Brønstad, B.M.; Nyhus, B.; Eriksson, M.; Aune, R.; Ren, X.; Akselsen, O.M.; Bunaziv, I. Additive Manufacturing with Superalloy Stainless Steel Wire by CMT Process. *Metals* **2020**, *10*, 272. [[CrossRef](#)]

49. Kaschel, F.R.; Celikin, M.; Dowling, D.P. Effects of laser power on geometry, microstructure and mechanical properties of printed Ti-6Al-4V parts. *J. Mater. Process. Technol.* **2020**, *278*, 116539. [[CrossRef](#)]
50. Liu, Y.; Wu, Z.; Liu, W.; Ma, Y.; Zhang, X.; Zhao, L.; Yang, K.; Chen, Y.; Cai, Q.; Song, Y.; et al. Microstructure evolution and reaction mechanism of continuously compositionally Ti/Al intermetallic graded material fabricated by laser powder deposition, *J. Mater. Res. Technol.* **2022**, *20*, 4173–4185. [[CrossRef](#)]

Disclaimer/Publisher's Note: The statements, opinions and data contained in all publications are solely those of the individual author(s) and contributor(s) and not of MDPI and/or the editor(s). MDPI and/or the editor(s) disclaim responsibility for any injury to people or property resulting from any ideas, methods, instructions or products referred to in the content.